Zonal Jets as Transport Barriers in Planetary Atmospheres

F. J. Beron-Vera, M. G. Brown, M. J. Olascoaga and I. I. Rypina*
Rosenstiel School of Marine and Atmospheric Science, University of Miami, Miami, Florida

H. Koçak
Departments of Computer Science and Mathematics, University of Miami, Coral Gables, Florida

I. A. Udovydchenkov*
Rosenstiel School of Marine and Atmospheric Science, University of Miami, Miami, Florida

Accepted for publication in the *Journal of the Atmospheric Sciences*.

(Started: April 13, 2007; this version: March 17, 2008.)

Corresponding author address:

F. J. Beron-Vera, RSMAS/AMP, University of Miami, 4600 Rickenbacker Cswy., Miami, FL 33149 (fberon@rsmas.miami.edu)

*Current affiliation: Woods Hole Oceanographic Institution, Woods Hole, Massachusetts.

ABSTRACT

The connection between transport barriers and potential vorticity (PV) barriers in PV-conserving flows is investigated with a focus on zonal jets in planetary atmospheres. A perturbed PV-staircase model is used to illustrate important concepts. This flow consists of a sequence of narrow eastward and broad westward zonal jets with a staircase PV structure; the PV-steps are at the latitudes of the cores of the eastward jets. Numerically simulated solutions to the quasigeostrophic PV conservation equation in a perturbed PV-staircase flow are presented. These simulations reveal that both eastward and westward zonal jets serve as robust meridional transport barriers. The surprise is that westward jets, across which the background PV gradient vanishes, serve as robust transport barriers. A theoretical explanation of the underlying barrier mechanism is provided. It is argued that transport barriers near the cores of westward zonal jets, across which the background PV gradient is small, are found in Jupiter's midlatitude weather layer and in the Earth's summer hemisphere subtropical stratosphere.

1. Introduction

In Rypina et al. (2007a) it was argued that the transport barrier near the core of the austral polar night jet can be explained by a mechanism different from the potential vorticity (PV) barrier mechanism (Juckes and McIntyre 1987). The new barrier mechanism, which was subsequently referred to as "strong KAM stability" (Rypina et al. 2007b), follows from an argument that does not make use of dynamical constraints on the streamfunction. This necessitates that dynamical constraints be considered separately. Interestingly, decoupling of the dynamical constraints from the barrier mechanism leads to the possibility that transport barriers in PV-conserving flows may occur at locations that do not coincide with PV-barriers. Rypina et al. (2007a) predicted that barriers of this type should be present in close proximity to the cores of westward zonal jets in planetary atmospheres. In this paper we demonstrate that transport barriers of this type are present in a numerically simulated PV-conserving flow. We also argue that barriers of the type described are present in Jupiter's midlatitude weather layer and in the Earth's summer hemisphere subtropical stratosphere.

In the following section passive tracer transport in a numerically simulated perturbed PV-staircase flow is investigated. It is shown that robust meridional transport barriers in close proximity to the cores of both eastward and westward zonal jets are present. The surprise is that westward jets, at which the background PV-gradient vanishes, act as transport barriers. Essential elements of the strong KAM stability argument are reviewed to explain this behavior. In section 3 we discuss the relevance of transport barriers of the strong KAM stability type to: 1) the interpretation of Jupiter's midlatitude weather layer belt-zone structure; and 2) the Earth's summer hemisphere subtropical stratosphere. In the final section we briefly discuss our results.

2. Transport barriers in a perturbed PV-staircase flow

In this section we consider passive tracer transport in a perturbed PV-staircase flow. We assume quasigeostrophic dynamics in a one-layer reduced-gravity setting and make use of a local Cartesian coordinate system (x, y) where x and y increase to the east and north, respectively, and the constant β is the local y-derivative of the Coriolis parameter. The zonal and meridional components of the velocity field are $u = -\partial\psi/\partial y$ and $v = \partial\psi/\partial x$, respectively, where $\psi(x, y, t)$ is the streamfunction. The flow is constrained to satisfy

$$\frac{\partial q}{\partial t} - \frac{\partial \psi}{\partial y}\frac{\partial q}{\partial x} + \frac{\partial \psi}{\partial x}\frac{\partial q}{\partial y} = 0 \tag{1}$$

where

$$q = \nabla^2\psi - L_{\mathrm{D}}^{-2}\psi + \beta y \tag{2}$$

is the quasigeostrophic potential vorticity and L_{D} is the deformation radius. Recent theoretical, numerical and experimental work, including extensions involving spherical geometry, shallow-water dynamics and inclusion of weak forcing and dissipation, has shown that flows satisfying (1)–(2) with periodic boundary conditions in x tend to evolve toward a state of the form

$$\psi = \psi_0(y) + \psi_1(x, y, t) \tag{3}$$

where ψ_1 is a small perturbation to ψ_0 (Cho and Polvani 1996; Danilov and Gryanik 2004; Danilov and Gurarie 2004; Dritschel and McIntyre 2008; Huang and Robinson 1998; Manfroi and Young 1999; Nozawa and Yoden 1997; Peltier and Stunhe 2002; Read et al. 2007; Rhines 1975; Scott and Polvani 2007; Vallis and Maltrud 1993; Williams 1978). The background zonal flow is characterized by an approximately piecewise constant PV distribution that has been appropriately described as a PV-staircase (Baldwin et al. 2007; Dritschel and McIntyre 2008; Dunkerton and Scott 2007). The

corresponding zonal velocity profile $u_0(y) = -\mathrm{d}\psi_0/\mathrm{d}y$ is periodic in y. Taking the period to be $2b$, the jump in $q_0(y)$ at each step is $2b\beta$, and the zonal flow is the periodic extension of

$$u_0(y) = \beta L_{\mathrm{D}}^2 \left(\frac{b}{L_{\mathrm{D}}} \frac{\cosh((y-b)/L_{\mathrm{D}})}{\sinh(b/L_{\mathrm{D}})} - 1 \right), \quad 0 \le y \le 2b, \tag{4}$$

consisting of a periodic sequence of alternating narrow eastward and broad westward zonal jets with $q_0(y)$ piecewise constant between adjacent eastward jets, as illustrated in Fig. 1. Note that at the center of each constant q_0 band lies a westward jet. In the limit $L_{\mathrm{D}}/b \to \infty$ (4) reduces to

$$u_0(y) = \frac{\beta}{2} \left((y-b)^2 - \frac{b^2}{3} \right), \quad 0 \le y \le 2b, \tag{5}$$

whose qualitative features are identical to those of the finite L_{D}/b case. The flows (4) and (5) are normalized so that the integral of $u_0(y)$ over y vanishes. The Rhines scale $\sqrt{U/\beta}$, where U is a characteristic velocity, is an approximate measure of the separation between adjacent eastward jets. Corresponding to (5) this separation is exactly $2b = 2\sqrt{3U_{\max}/\beta}$ where $U_{\max}$ is the wind speed at the core of one of the eastward jets.

Before presenting numerical simulations of passive tracer transport in a perturbed PV-staircase flow we describe predictions based on two different arguments of the expected locations of transport barriers in this flow. First, the PV-barrier argument (Dritschel and McIntyre 2008) leads to the expectation that transport barriers should be present only near the cores of the eastward jets. The basic elements of the PV-barrier argument were used originally by Juckes and McIntyre (1987) to explain the mechanism by which the eastward jet at the perimeter of the austral stratospheric polar vortex, sometimes referred to as the austral polar night jet, during the late winter and early spring serves to trap ozone-depleted air inside the polar vortex. The essential elements of the argument are that at eastward jets the large gradient of $q_0(y)$ is associated

with a large Rossby wave restoring force ("Rossby wave elasticity") which inhibits meridional exchange of fluid at larger scales and that shear $u_0'(y) = \mathrm{d}u_0/\mathrm{d}y$ acts to inhibit meridional exchange at smaller scales. (But note that in Rypina et al. (2007a) it is argued that increasing meridional shear acts, on average, to increase meridional exchange.)

An alternative argument, based on the strong KAM stability mechanism (Rypina et al. 2007a, b), leads to the expectation that transport barriers should be present near the cores of both eastward and westward jets in a PV-staircase flow. The argument leading to this expectation will now be reviewed. The Lagrangian (particle trajectory) equations of motion,

$$\frac{\mathrm{d}x}{\mathrm{d}t} = -\frac{\partial \psi}{\partial y}, \quad \frac{\mathrm{d}y}{\mathrm{d}t} = \frac{\partial \psi}{\partial x}, \tag{6}$$

constitute a nonautonomous one-degree-of-freedom Hamiltonian system, with (x, y) the canonically conjugate coordinate–momentum pair and $\psi(x, y, t)$ the Hamiltonian. This allows results from studies of integrable and nonintegrable Hamiltonian systems to be applied. In the background steady flow, with $\psi = \psi_0(y)$, equations (6) are integrable and the motion is describable using a transformed Hamiltonian $H_0(I)$ where (I, θ) are action–angle variables. Each trajectory lies on a torus which is labeled by its I-value. Motion is 2π-periodic in θ with angular frequency $\omega(I) = H_0'(I)$. According to each of many variants of the Kolmogorov–Arnold–Moser (KAM) theorem (Arnold et al. 1986), many of the unperturbed tori survive in the perturbed system (3), albeit in a slightly distorted form, provided certain conditions are met. Surviving tori cannot be traversed and serve as transport barriers. (For reasons described in (Rypina et al. 2007a), the process known as Arnold diffusion does not occur in the systems under study.) Torus destruction is caused by the excitation and overlapping of resonances. Each resonance has a characteristic width $\Delta\omega$. Nondegenerate $\omega'(I) \neq 0$ resonance widths are proportional to $|\omega'(I)|^{1/2}$. Degenerate $\omega'(I) = 0$ resonance widths do not vanish but

are generally narrower than nondegenerate resonance widths. (Quantitative estimates of both degenerate and nondegenerate resonance widths are given in (Rypina et al. 2007b); for our purposes it suffices to note the general trend.) For most moderate strength perturbations to the background, small resonance widths near degenerate tori lead to nonoverlapping resonances and thus unbroken tori that serve as transport barriers. This constitutes the strong KAM stability barrier argument. In our model (3) the connection between (x, y) and (I, θ) is particularly simple: $I = -Ry/(2\pi)$, $\theta = 2\pi x/R$ where R is the distance around the planet along a constant latitude circle at the latitude at which β is defined. The period of motion $2\pi/\omega$ is $R/u_0(y)$, so $\omega(I) = 2\pi R^{-1} u_0(-I/R)$. At the cores of both eastward and westward jets $u_0'(y) = 0$, so $\omega'(I) = 0$ at these locations and the strong KAM stability argument predicts that robust meridional transport barriers should be present. Barriers of this type may be broken if the transient perturbation $\psi_1(x, y, t)$ strongly excites a low-order resonance with the frequency $\omega = 2\pi u_0(y)/R$ of the background flow near the core of the jet. Three final issues are noteworthy. First, because the strong KAM stability argument is a kinematic argument (based on (6) alone), dynamical consistency—consistency between (1)–(3) and (4) or (5)—and flow stability must be considered separately. Second, our emphasis on jets is unnecessarily restrictive inasmuch as the strong KAM stability argument holds at all locations where $u_0'(y) = 0$. Third, the stated results on KAM theory assume that $\psi_1(x, y, t)$ can be expressed as a multiperiodic (generically quasiperiodic) function of t.

We now describe a set of numerical experiments that were performed to investigate passive tracer transport in a perturbed PV-staircase flow. The streamfunctions on which our tracer transport simulations are based were constructed by numerically solving (1)–(2) using as an initial state a perturbation to the background PV-staircase (4). Before presenting the results, it is appropriate to make two comments about what we expect to learn from these simulations. First, these simulations provide a test of the assertion that the decomposition (1)–(4) is dynamically consistent. Second,

given a positive outcome of the first test, these simulations test whether westward zonal jets, across which there is no PV-barrier, serve as robust meridional transport barriers. The quasigeostrophic equation (1)–(2) was solved numerically using a standard pseudospectral technique on a 256^2 grid in the $[0, 8b) \times [-4b, 4b)$ computational domain. Periodic boundary conditions in ψ were applied in both the x and y directions. The Arakawa representation of the advective terms, which are often written as a Jacobian, was used. The solution was marched forward in time using a second-order Adams–Bashforth scheme with a dimensionless timestep $\beta b \Delta t = 0.002$. To control the spurious amplification of high wavenumber modes, we applied a weak exponential cutoff filter and included a small amount of hyperviscosity. Two types of initial perturbation to the background PV-staircase were used in our simulations. The first type of perturbation consisted of a superposition of periodic displacements of PV contours with random phases uniformly distributed on $[0, 2\pi)$. The second type of perturbation was a doubly periodic perturbation to the streamfunction consisting of a sum of a product of Fourier modes with random phases. In all of our simulations the separation between adjacent eastward jets $2b$ was taken to be 8000 km and $\beta = 3.442 \times 10^{-9}$ km^{-1} s^{-1} was used. The simulations shown correspond to $L_{\rm D} = b/2$. In anticipation of our discussion of Jupiter in the following section, these parameters were chosen to approximately reproduce conditions on Jupiter. Note, however, that in our simulations the period in x is 32000 km, which is approximately one-tenth the midlatitude distance around Jupiter on a line of constant latitude. Many one-year model simulations were run. For some parameter values ten-year model simulations were performed. For the parameter values given, the change in both energy and enstrophy throughout the duration of the simulations performed was less than 1%, giving us confidence in the accuracy of the simulations. Both types of initial perturbation gave similar results.

FIG. 1.

Figure 2 shows plots of instantaneous, at $t = \tau = 1$ year, zonally-averaged zonal velocity $\bar{u}(y, \tau)$, zonally averaged potential vorticity $\bar{q}(y, \tau)$ and potential vorticity

$q(x, y, \tau)$. Comparison of Figs. 1 and 2 provides strong support for the dynamical consistency of the decomposition (3)–(4), but these plots provide no insight into whether transport barriers are present. To address the latter question we have used the year-long records of computed velocity fields to: 1) follow the evolution of distributions of passive tracers, which evolve according to (6); and 2) compute finite-time Lyapunov exponents (FTLEs; see, for example, Haller 2001). Typical results are shown in Fig. 3. As shown in the figure, the initial positions of the passive tracers fell on the lines $\pm 2y/b = \{1, 3, 5, 7\}$, which lie midway between the unperturbed eastward and westward jets. It is seen that after a one-year integration the regions between jets are well-mixed, but that there is no meridional transport across the cores of the zonal jets. It should be emphasized that in this and other simulations tracer particles spread meridionally to fill the domains shown in about two weeks. Throughout the reminder of the one-year integration no additional meridional tracer spreading occurs. With this in mind, Fig. 3 clearly shows that both eastward and westward zonal jets act as meridional transport barriers, consistent with the strong KAM stability argument. Calculation of FTLEs provides an additional test of the correctness of the strong KAM stability argument. Lyapunov exponents are a measure of the rate of divergence of neighboring trajectories. According to the strong KAM stability argument, the transport barriers at the cores of zonal jets coincide with generally thin bands of KAM invariant tori on which Lyapunov exponents are zero. Finite time estimates of Lyapunov exponents will not be identically zero on KAM invariant tori, but these structures should be readily identifiable as thin bands of low FTLE estimates. This is precisely what is seen in Fig. 3; both westward and eastward jets are identifiable as thin bands of low FTLE estimates, consistent with the strong KAM stability argument. Typical computed values of FTLE, in units of $10^{-3}\beta b$, shown in Fig. 3 are 2 at the cores of the westward jets, 7 at the cores of the eastward jets, and 17 in the well-mixed regions.

FIG. 2.

We have performed many numerical experiments based on PV-staircase flows of

FIG. 3.

the type described here. These simulations support the conclusion that both eastward zonal jets (where $\partial\bar{q}/\partial y$ is very large) and westward zonal jets (where $\partial\bar{q}/\partial y$ is very small) act as robust meridional transport barriers. This conclusion is not sensitive to the choice of parameter values or details of the initial perturbation. Two general trends are noteworthy. First, for a small perturbation the width of the barrier region near westward jets is greater than the width of the barrier region near eastward jets. This behavior is consistent with the strong KAM stability argument: $|\omega'(I)|$ is small over a larger y-domain near westward jets than near eastward jets. Second, as the perturbation strength increases, transport barriers near westward jets generally break before eastward jet barriers break. In our simulations the westward jet barriers broke when the initial rms meridional PV-contour displacement exceeded approximately $b/4$, while the eastward jet barriers broke when the initial rms displacement was approximately twice this value. Possible explanations for the somewhat more robust nature of the eastward jets are: 1) the PV-barrier mechanism and the strong KAM stability barrier mechanism act in tandem to strengthen the barriers near eastward jets; and 2) we have performed a linear theory Rossby wave analysis of PV-staircase flows that reveals that Rossby wave critical layers are precluded at the eastward jets (see also Dunkerton and Scott 2007), which suggest that the eastward jet barriers may be more robust.

3. Observational evidence from planetary atmospheres

In the previous section it was demonstrated that transport barriers may exist in a PV-conserving flow at locations that do not coincide with PV-barriers. In this section we discuss observational evidence that suggests the existence of transport barriers in the absence of PV-barriers. We consider two examples: 1) Jupiter's weather layer; and 2) the Earth's stratosphere. In both cases, conclusions drawn should be regarded as tentative inasmuch as we do not treat either system in enough depth to make a definitive statement. In spite of our incomplete treatment of these topics,

we feel that it is important to point out that, consistent with the theoretical and numerical results presented in the previous section, there is observational evidence in planetary atmospheres that suggests the existence of transport barriers in the absence of PV-barriers that can be explained by the strong KAM stability mechanism. Both the examples considered are, in our view, sufficiently important that the connection between the observations discussed and the strong KAM stability barrier mechanism is worthy of a much more thorough investigation.

It is natural to focus on flows consisting of a sequence of alternating eastward and westward zonal jets because many of the arguments used in the previous section are then applicable. In particular, for this class of flows, meridional transport barriers of the strong KAM stability type are predicted to occur at the latitudes where $u_0'(y) = 0$. Furthermore, in alternating zonal jet flows one may anticipate that eastward and westward jets are associated with large and small background PV-gradients, respectively. Note, however, that for the purpose of identifying transport barriers in the absence of PV-barriers it is not necessary that the background PV distribution in the flows considered be that of an idealized PV-staircase. This point is discussed in more detail below. The following simple scaling argument shows why an alternating zonal jet flow is well-developed in Jupiter's weather layer but is only marginally identifiable in the Earth's stratosphere. These systems are then discussed in turn.

Recall that in a PV-staircase flow the separation between adjacent eastward jets is $2b = 2\sqrt{3U_{\max}/\beta}$. We shall assume that this estimate approximately holds for general midlatitude multiple zonal jet mean flow patterns. Let r denote planetary radius and Ω planetary rotation rate. Then $\beta \sim \Omega/r$ and the number of eastward (or westward) jets one expects to observe in each hemisphere at midlatitudes (whose extent in latitude is taken here to be half the equator to pole distance) is approximately $n_{\rm jet} \sim \frac{\pi}{4} r/(2\sqrt{3U_{\max} r/\Omega}) \sim \frac{1}{4}\sqrt{\Omega/(U_{\max} r)}$. In Jupiter's weather layer ($U_{\max} \sim 50$ m s^{-1}, $r \sim 7 \times 10^4$ km, $\Omega \sim 2\pi/10$ h) $n_{\rm jet} \sim 5$, in good agreement with Fig. 4, as

described below. In the Earth's stratosphere ($U_{\max} \sim 50$ m s^{-1}, $r \sim 6.4 \times 10^3$ km, $\Omega \sim 2\pi/24$ h) $n_{\rm jet} \sim 1$. Thus, conditions for the formation of a multiple zonal jet mean flow pattern are only marginally satisfied in the Earth's stratosphere. In the Earth's troposphere $U_{\max}$ is smaller, suggesting more favorable conditions, but mountain ranges and thermal exchange processes between the atmosphere and irregularly shaped oceans and continents constitute significant hindrances to the formation of zonal flows. Conditions are favorable in the Earth's oceans ($U_{\max} \sim 0.5$ m s^{-1}, corresponding to $n_{\rm jet} \sim 8$) but there the presence of lateral boundaries dictates that zonal jets be embedded in recirculation gyres (Maximenko et al. 2005, 2008; Richards et al. 2006).

a. Jupiter's weather layer

The most striking feature of Jupiter's weather layer circulation (Porco et al. 2003; Vasavada and Showman 2005) is that it is organized in a sequence of alternating eastward and westward zonal jets whose meridional excursion is very small. Figure 4 shows zonally-averaged zonal wind speed on Jupiter at the cloud top level as a function of latitude. Regions with dark and light shading in this figure are referred to as belts and zones, respectively. Belts and zones correspond to regions in which the background motion is cyclonic ($u_0'(y) < 0$) and anticyclonic ($u_0'(y) > 0$), respectively. The boundaries between adjacent belts and zones coincide with the cores of the zonal jets. At these boundaries $u_0'(y) = 0$. Belts and zones have different radiative transfer properties (analyses are not limited to the visible band of the electromagnetic spectrum) which is attributed to differences in chemical composition (Banfield et al. 1998; Carlson et al. 1994; Irwin et al. 2005; Irwin et al. 2001; Simon-Miller et al. 2001). Assuming that the weather layer flow is approximately two dimensional and that chemical species are long-lived, one may infer from the observation that adjacent belts and zones have different chemical constituents that there is very little fluid exchange between adjacent belts and zones, implying that both eastward and westward zonal jets act as robust

meridional transport barriers. FIG. 4.

Figure 5 shows $u_0(y)$, $q_0(y)$, and $q_0'(y)$ in Jupiter's weather layer. The same data are shown (but are plotted differently) in Read et al. (2006). The question of whether a PV-staircase is a useful approximate model of Jupiter's weather layer has been considered by many authors (Dowling 1995; Marcus and Lee 1998; Peltier and Stunhe 2002; Read et al. 2006). For our purposes the answer to this question is not critical. Our focus is on identifying transport barriers that cannot be explained by the PV-barrier mechanism. Figure 5 shows that while all eastward jets are associated with large meridional PV-gradients, most of the westward jets are associated with small meridional PV-gradients. (Here and above we are using the term westward jet somewhat loosely to include minima of $u_0(y)$, even when $u_0 > 0$ at the minimum.) In other words, most of the transport barriers near the cores of the westward jets cannot be explained by the PV-barrier mechanism. But all of the belt-zone boundaries—the apparent meridional transport barriers—coincide with latitudes at which $u_0'(y) = 0$, consistent with the strong KAM stability barrier mechanism. Thus all of the apparent transport barriers can be explained by the strong KAM stability barrier mechanism. Note, however, that there is no apparent barrier on the equator, where $u_0'(y) = 0$. This is probably due to a combination of anomalous equatorial dynamics (Heimpel et al. 2005) and the manner by which chemical constituents are pumped into the near-equatorial weather layer. FIG. 5.

Some caveats relating to our interpretation of observations from Jupiter should be emphasized, however. First, we have assumed that the weather layer flow is nearly two dimensional and horizontally nondivergent, being only weakly forced by convection. Although these assumptions are generally accepted (see, for example, Vasavada and Showman 2005), it should be noted that our explanation of the apparent transport barrier rests on their validity. A second assumption that we have made is that chemical species in Jupiter's weather layer are long-lived. Another possible explanation of the apparent transport barriers between adjacent belts and zones is that chemical

species are short-lived, being continuously pumped into the weather layer by convective overturning (Ingersoll et al. 2000; Showman and de Pater 2005). We cannot rule out this possibility. Our argument shows, however, that the apparent lack of fluid exchange between adjacent belts and zones *can* be explained using dynamical arguments.

b. The Earth's stratosphere

The simple scaling argument given above predicts that conditions for the formation of a stable alternating multiple jet zonal mean flow pattern are only marginally satisfied in the Earth's stratosphere. In qualitative agreement with this prediction, in each hemisphere there is one readily identifiable eastward zonal jet and one westward jet, and the appearance of these jets is seasonal (see, for example, Andrews et al. 1987). The stronger jets are the high latitude eastward polar night jets which appear in the winter hemisphere. (The austral polar night jet is particularly strong, persisting throughout most of the stratosphere during the austral fall, winter and spring.) The westward jets are present in the subtropics throughout most of the stratosphere during the summer months in each hemisphere. The eastward polar night jets, especially in the southern hemisphere, act as transport barriers and are associated with strong PV-gradients. Because the focus in the present study is on identifying transport barriers in the absence of PV-barriers, these jets are not of interest here. In contrast, the westward subtropical jets in the summer hemisphere are very much of interest because these are not associated with a strong PV-gradient. The properties just described are illustrated in Fig. 6. That figure shows a 7-year (1992–1998) monthly average of zonally-averaged potential vorticity (in color) and zonal wind (as contours) on the 460 K isentropic surface (which lies in the lower stratosphere) based on the European Center for medium-Range Weather Forecasts (ECMWF) 40-year Re-Analysis (ERA-40) product. Both the eastward polar night jets and the westward subtropical jets are readily identifiable. As we have noted, the eastward winter hemisphere polar night jets

are associated with strong meridional PV-gradients while the westward subtropical jets are associated with nearly homogenous PV-distributions. The westward subtropical jets have the dynamical properties that we seek—zonal jets in the absence of strong PV-gradients. We note also that, consistent with arguments made originally by Charney and Drazin (1961), Rossby wave perturbations to the background in these regions are weak. From the standpoint of applicability of the strong KAM stability argument, weak perturbations are advantageous. FIG. 6.

We turn our attention now to the question of whether the cores of these jets serve as robust meridional transport barriers. Studies of stratospheric transport based on effective diffusivity have been carried out by Allen and Nakamura (2001) and Haynes and Shuckburgh (2000). The effective diffusivity is large (small) in regions where fluid is well (poorly) mixed. Fluid in the vicinity of a transport barrier is poorly mixed; these regions are thus characterized by a small effective diffusivity. Both stratospheric effective diffusivity analyses reveal that the westward subtropical jet in the summer hemisphere coincides with a region of anomalously low effective diffusivity; see plates 1 and 4 in Allen and Nakamura (2001) and 1 through 4 in Haynes and Shuckburgh (2000). This suggests that these westward jets act as meridional transport barriers. Previous work by Waugh (1996) and Chen et al. (1994) had focused on this "subtropical barrier." Indeed, this barrier comprises a critical element of the "tropical pipe" model (Plumb 1996) of stratospheric transport. Observational evidence that suggests the presence of subtropical transport barriers is presented in Grant et al. (1996), Mote et al. (1998), Minschwaner et al. (1996), Trepte and Hitchman (1992) and Trepte et al. (1993). Shepherd (2007) provides a recent review of stratospheric transport, including a discussion of subtropical transport barriers.

The evidence that we have pointed out strongly suggests that: 1) the stratospheric subtropical barrier is a robust meridional transport barrier that coincides with the core of a westward jet; 2) the associated meridional PV-gradient is very small so this barrier

cannot be explained by the PV-barrier mechanism; and 3) because $u_0'(y) = 0$ at this barrier, the barrier is predicted by the strong KAM stability barrier mechanism. To test these tentative conclusions more rigorously, a study based on realistic synoptic winds that tracks both potential vorticity and tracer distributions should be conducted.

4. Summary and discussion

In the first part of this paper we presented numerical simulations of passive tracer transport in a perturbed PV-staircase flow and showed that both eastward and westward jets in this flow act as meridional transport barriers. The surprise is that westward jets, where the background PV gradient vanishes, act as transport barriers. This behavior was explained as being a consequence of the strong KAM stability barrier mechanism.

We then briefly discussed the applicability of the strong KAM stability mechanism to explaining observations of Jupiter's weather layer and the Earth's subtropical stratosphere. In both of these systems westward jets are present that appear to act as robust meridional transport barriers in the absence of a background meridional PV-barrier. These barriers are predicted by the strong KAM stability mechanism. In both cases the evidence presented should be regarded as suggestive. More thorough investigations of both problems is recommended.

The principal weakness of our explanation of the apparent lack of fluid exchange between adjacent belts and zones in Jupiter's midlatitude weather layer is that we cannot exclude the possibility that the observed chemical composition differences in adjacent belts and zones are caused by a combination of strong convective overturning and short-lived chemical species. In spite of this caveat, it is important to emphasize that we have shown that maintenance of the apparent chemical composition differences between adjacent belts and zones *can* be explained using a dynamical argument (as opposed to a chemistry-based argument) in which the weather layer flow is only weakly convectively forced.

The principal weaknesses in our discussion of the Earth's subtropical stratospheric transport barrier were that all of the properties noted were based on averaged winds rather than synoptic winds and that tracer transport and potential vorticity distributions were not estimated in a way that was guaranteed to be self consistent. It should not be difficult to overcome these shortcomings using model-based synoptic winds.

Acknowledgments. We thank T. Dowling and R. Morales-Juberias for providing the data used to construct Figs. 4 and 5. Comments on the manuscript by anonymous reviewers, T. Shepherd, T. Özgökmen, and J. Willemsen are sincerely appreciated. The ECMWF ERA-40 data used in this study were obtained from the ECMWF data server. Support for this work was provided by the U.S. National Science Foundation under grants CMG0417425 and OCE0648284.

REFERENCES

Allen, R. A., and N. Nakamura, 2001: A seasonal climatology of effective diffusivity in the stratophere. *J. Geophys. Res.*, **106**, 7917–7935.

Andrews, D. G., J. R. Holton, and C. B. Leovy, 1987: *Middle Atmosphere Dynamics*. vol. 40 of *International Geophysical Series*, Academic.

Arnold, V. I., V. V. Kozlov, and A. I. Neistadt, 1986: *Mathematical Aspects of Classical and Celestial Mechanics*. vol. 3 of *Encyclopedia of Mathematical Sciencies*, Springer.

Baldwin, M. P., P. B. Rhines, H.-P. Huang, and M. E. McIntyre, 2007: The jet-stream conundrum. *Science*, **315**, 467–468.

Banfield, D., P. J. Gierasch, M. Bell, E. Ustinov, A. P. Ingersoll, A. R. Vasavada, R. A. West, and M. J. S. Belton, 1998: Jupiter's Cloud Structure from Galileo Imaging Data. *Icarus*, **135**, 230–250.

Carlson, B. E., A. A. Lacis, and W. B. Rossow, 1994: Belt-zone variations in the Jovian cloud structure. *J. Geophys. Res.*, **99**, 14,623–14,658.

Charney, J. G., and P. G. Drazin, 1961: Propagation of planetary-scale disturbances from the lower into the upper atmosphere. *J. Geophys. Res.*, **66**, 83–109.

Chen, P., J. R. Holton, A. O'Neil, and R. Swinbank, 1994: Isentropic mass exchange between tropics and extratropics in the stratosphere. *J. Geophys. Res.*, **51**, 3006–3018.

Cho, J. Y.-K., and L. Polvani, 1996: The emergence of zonal jets and vortices in freely evolving, shallow-water turbulence on a sphere. *Phys. Fluids*, **8**, 1531–1552.

Danilov, S., and V. M. Gryanik, 2004: Barotropic beta-plane turbulence in a regime with strong zonal jets revisited. *J. Atmos. Sci.*, **61**, 2283–2295.

Danilov, S., and D. Gurarie, 2004: Scaling, spectra and zonal jets in beta-plane turbulence. *Phys. Fluids*, **16**, 2592–2603.

Dowling, T. E., 1995: Dynamics of Jovian Atmospheres. *Annu. Rev. Fluid Mech.*, **27**, 293–334.

Dritschel, D. G., and M. E. McIntyre, 2008: . Multiple jets as PV staircases: the Phillips effect and the resilience of eddy-transport barriers, *J. Atmos. Sci.*, in press.

Dunkerton, T. J., and R. K. Scott, 2007: . A barotropic model of the angular momentum conserving potential vorticity staircase in spherical geometry, *J. Atmos. Sci.*, in press.

Grant, W. B., E. V. Browell, C. S. Long, L. L. Stowe, R. G. Grainger, and A. Lambert, 1996: Use of volcanic aerosols to study the tropical stratospheric reservoir. *J. Geophys. Res.*, **101**, 3973–3988.

Haller, G., 2001: Lagrangian structures and the rate of starin in a partition of two-dimensional turbulence. *Phys. Fluids*, **13**, 3365–3385.

Haynes, P., and E. Shuckburgh, 2000: Effective diffusivity as a diagnostic of atmospheric transport 1. Stratosphere. *J. Geophys. Res.*, **105**, 22,777–22,794.

Heimpel, M., J. J. Aurnou, and Wicht, 2005: Simulation of equatorial and high-latitude jets on Jupiter in a deep convection model. *Nature*, **438**, 193–196.

Huang, H. P., and W. A. Robinson, 1998: Two-dimensional turbulence and persistent zonal jets in a global barotropic model. *J. Atmos. Sci.*, **55**, 611–632.

Ingersoll, A. P., P. J. Gierasch, D. Banfield, A. R. Vasavada, and the Galileo Imaging Team, 2000: Moist convection as an energy source for the large-scale motions in Jupiter's atmosphere. *Nature*, **403**, 630–632.

Irwin, P. G. J., K. Sihra, N. Bowles, F. W. Taylor, and S. B. Calcutt, 2005: Methane absorption in the atmosphere of Jupiter from 1800 to 9500 cm^{-1} and implications for vertical cloud structure. *Icarus*, **176**, 255–271.

Irwin, P. G. J. I., A. L. Weir, F. W. Taylor, S. B. Calcutt, and R. W. Carlson, 2001: The origin of belt/zone contrasts in the atmosphere of Jupiter and their correlation with 5-mu m opacity. *Icarus*, **149**, 397–415.

Juckes, N. M., and M. E. McIntyre, 1987: A high-resolution one-layer model of breaking planetary waves in the stratosphere. *Nature*, **328**, 590–596.

Manfroi, A. J., and W. R. Young, 1999: Slow evolution of zonal jets on the beta plane. *J. Atmos. Sci.*, **56**, 784–800.

Marcus, P. S., and C. Lee, 1998: A model for eastward and westward jets in laboratory experiments and planetary atmospheres. *Phys. Fluids*, **10**, 1474–1489.

Maximenko, A. N., B. Bang, and H. Sasaki, 2005: Observational evidence of alternating zonal jets in the world ocean. *Geophys. Res. Lett.*, **32**, L12,607.

Maximenko, A. N., O. V. Melnichenko, and a. H. S. P. P. Niiler, 2008: Stationary mesoscale jet-like features in the ocean, *Geophys. Res. Lett.*, in press.

Minschwaner, K., A. E. Dessler, J. W. Elkins, C. M. Volk, D. W. Fahey, M. Loewenstein, J. R. Podolske, A. E. Roche, and K. R. Chan, 1996: Bulk properties of isentropic mixing into the tropics in the lower stratosphere. *J. Geophys. Res.*, **101**, 9433–9440.

Mote, P. W., T. J. Dunkerton, M. E. McIntyre, E. A. Ray, P. H. Haynes, and J. M. Russell, 1998: Vertical velocity, vertical diffusion, and dilution by midlatitude air in the tropical lower stratosphere. *J. Geophys. Res.*, **103**, 8651–8666.

Nozawa, T., and S. Yoden, 1997: Formation of zonal bands structure in forced two-dimensional turbulence on a rotating sphere. *Phys. Fluids*, **9**, 3129–3132.

Peltier, W. K., and G. R. Stunhe, 2002: The upscale turbulent cascade: shear layers, cyclones and gas giant bands. *Meteorology at the Millennium*, R. P. Pierce, Ed., Academic.

Plumb, R. A., 1996: A "tropical pipe" model of stratospheric transport. *J. Geophys. Res.*, **101**, 3957–3972.

Porco, C. C., et al., 2003: Cassini imaging of Jupiter's atmosphere, satellites, and rings. *Science*, **299**, 1541–1547.

Read, P. L., P. J. Gierasch, B. J. Conrath, A. Simon-Miller, T. Fouchet, and Y. H. Yamazaki, 2006: Mapping potential-vorticity dynamics on Jupiter. I: Zonal-mean circulation from Cassini and Voyager 1 data. *Q. J. R. Meteorol. Soc.*, **132**, 1577–1603.

Read, P. L., Y. H. Yamazaki, S. R. Lewis, P. D. Williams, R. Wordsworth, K. Miki-Yamazaki,

J. Sommeria, and H. Didelle, 2007: Dynamics of convectively driven banded jets in the laboratory. *J. Atmos. Sci.*, **64**, 4031–4052.

Rhines, P. B., 1975: Waves and turbulence on a beta-plane. *J. Fluid Mech.*, **69**, 471–443.

Richards, K. J., N. A. Maximenko, F. O. Bryan, and H. Sasaki, 2006: Zonal jets in the Pacific Ocean. *Geophys. Res. Lett.*, **33**, L03,605.

Rypina, I. I., M. G. Brown, F. J. Beron-Vera, H. Kocak, M. J. Olascoaga, and I. A. Udovydchenkov, 2007a: On the Lagrangian dynamics of atmospheric zonal jets and the permeability of the stratospheric polar vortex. *J. Atmos. Sci.*, **64**, 3595–3610.

Rypina, I. I., M. G. Brown, F. J. Beron-Vera, H. Kocak, M. J. Olascoaga, and I. A. Udovydchenkov, 2007b: Robust transport barriers resulting from strong Kolmogorov–Arnold–Moser stability. *Phys. Rev. Lett.*, **98**, 104,102.

Scott, R. K., and L. M. Polvani, 2007: Forced-dissipative shallow-water turbulence on the sphere and the atmospheric circulation of the giant planets. *J. Atmos. Sci.*, **64**, 3158–3176.

Shepherd, T. G., 2007: Transport in the middle atmosphere. *J. Met. Sot. Japan*, **85B**, 165–191.

Showman, A. P., and I. de Pater, 2005: Dynamical implications of Jupiter's tropospheric ammonia abundance. *Icarus*, **174**, 192–204.

Simon-Miller, A. A., D. Banfield, and P. J. Gierasch, 2001: Color and the vertical structure in Jupiter's belts, zones, and weather systems. *Icarus*, **154**, 459–474.

Trepte, C. R., and M. H. Hitchman, 1992: Tropical stratospheric circulation deduced from satellite aerosol data. *Nature*, **355**, 626–628.

Trepte, C. R., R. E. Veiga, and M. P. McCormick, 1993: The poleward dispersal of Mount Pinatubo volcanic aerosol. *J. Geophys. Res.*, **98**, 18,563–18,574.

Vallis, G. K., and M. E. Maltrud, 1993: Generation of mean flows and jets on a beta plane and over topography. *J. Phys. Oceanogr.*, **23**, 1346–1362.

Vasavada, A. R., and A. P. Showman, 2005: Jovian atmospheric dynamics: an update after Galileo and Cassini. *Rep. Prog. Phys.*, **68**, 1935–1996.

Waugh, D. W., 1996: Seasonal variation of transport out of the tropical stratosphere. *J. Geophys. Res.*, **101**, 4007–4023.

Williams, G. P., 1978: Planetary circulations 1: Barotropic representations of Jovian and terrestrial turbulence. *J. Atmos. Sci.*, **35**, 1399–1426.

Printed March 19, 2008.

Figure Captions

FIG. 1. Zonal velocity (left panel) and potential vorticity (right panel) in a PV-staircase zonal flow. The zonal velocity structure shown corresponds to the finite $L_{\rm D}$ case, Eq. (4), with $L_{\rm D} = b/2 = 2000$ km, roughly approximating midlatitude conditions on Jupiter. In this figure the ideal PV jumps have smooth transition regions with tanh dependence on y locally.

FIG. 2. Instantaneous zonally-averaged zonal velocity (left panel), zonally-averaged potential vorticity (middle panel), and potential vorticity (right panel) after a one-year simulation of the quasigeostrophic equation (1)–(2) using as initial state a perturbation to the PV-staircase flow of Fig. 1.

FIG. 3. (a) Zonally averaged zonal velocity $\bar{u}(y)$ at $t = 1$ year. (b) Initial positions $(x(0), y(0))$ of color-coded passive tracers. (c) Positions $(x(\tau), y(\tau))$ of color coded passive tracers at $t = \tau = 1$ year . (d) Finite-time Lyapunov exponent (FTLE) field as a function of initial position computed using a one year integration time interval. The time-dependent velocity field whose final state is shown in Fig. 2 was used to construct (a), (c) and (d).

FIG. 4. (left panel) Zonally-averaged zonal wind speed as a function of latitude on Jupiter at the cloud top level as inferred from images taken in December 2000 by the *Cassini* spacecraft (Porco et al. 2003). Gray and white zonal bands indicate belts and zones, respectively. (right panel) Near instantaneous visible band image of Jupiter constructed from images taken by the *Cassini* spacecraft in December 2000. Note that many features of Jupiter's weather layer that are not seen in this image may be revealed by radiative transfer analyses outside of the visible band of the electromagnetic spectrum. NASA image PIA07782 (PIA images are available at NASA's Planetary Photojournal website http://photojournal.jpl.nasa.gov).

FIG. 5. Meridional distribution of zonally-averaged zonal wind $u_0(y)$ (left panel), zonally-averaged potential vorticity $q_0(y)$ (center panel), and zonally-averaged potential vorticity gradient $q_0'(y)$ (right panel) in Jupiter's weather layer based on *Cassini* data. Both unsmoothed and smoothed wind profiles are plotted; the smoothed wind profile was used to compute $q_0(y)$ and $q_0'(y)$. Solid and dashed horizontal lines are drawn at the latitudes of the cores of westward and eastward jets, respectively. Note that large positive values of $q_0'(y)$ coincide with the cores of eastward jets. A spherical planet (rather than a β-plane, which is used elsewhere in this paper) was assumed to compute the $q_0(y)$ and $q_0'(y)$ structures shown.

FIG. 6. Seven-year (1992–1998) monthly average of zonally-averaged zonal wind and potential vorticity on the 460 K isentropic surface based on the ERA-40 reanalysis product. Contours show zonal winds in meters per second. Solid and dashed contours represent eastward and westward flow, respectively. Colors indicate Ertel's potential vorticity.

Figures

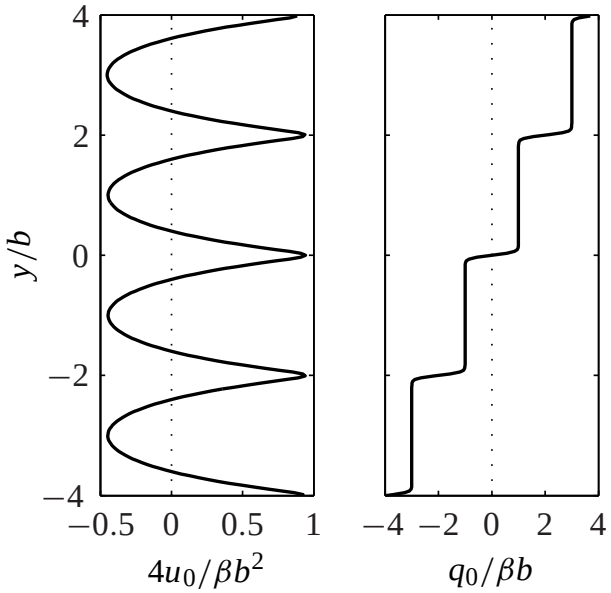

FIG. 1. Zonal velocity (left panel) and potential vorticity (right panel) in a PV-staircase zonal flow. The zonal velocity structure shown corresponds to the finite L_{D} case, Eq. (4), with $L_{\mathrm{D}} = b/2 = 2000$ km, roughly approximating midlatitude conditions on Jupiter. In this figure the ideal PV jumps have smooth transition regions with tanh dependence on y locally.

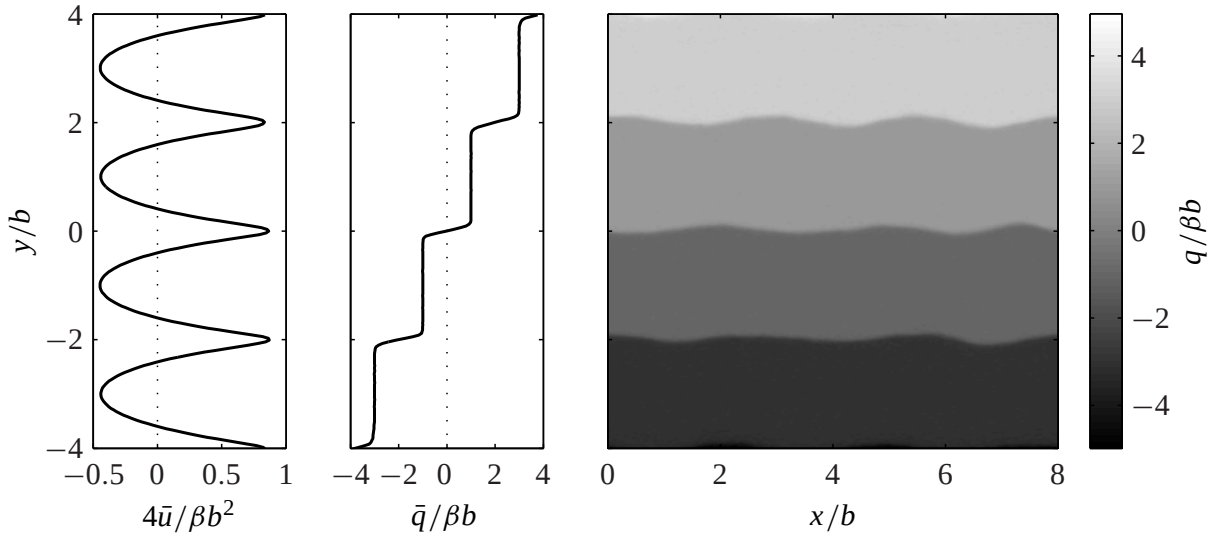

FIG. 2. Instantaneous zonally-averaged zonal velocity (left panel), zonally-averaged potential vorticity (middle panel), and potential vorticity (right panel) after a one-year simulation of the quasigeostrophic equation (1)–(2) using as initial state a perturbation to the PV-staircase flow of Fig. 1.

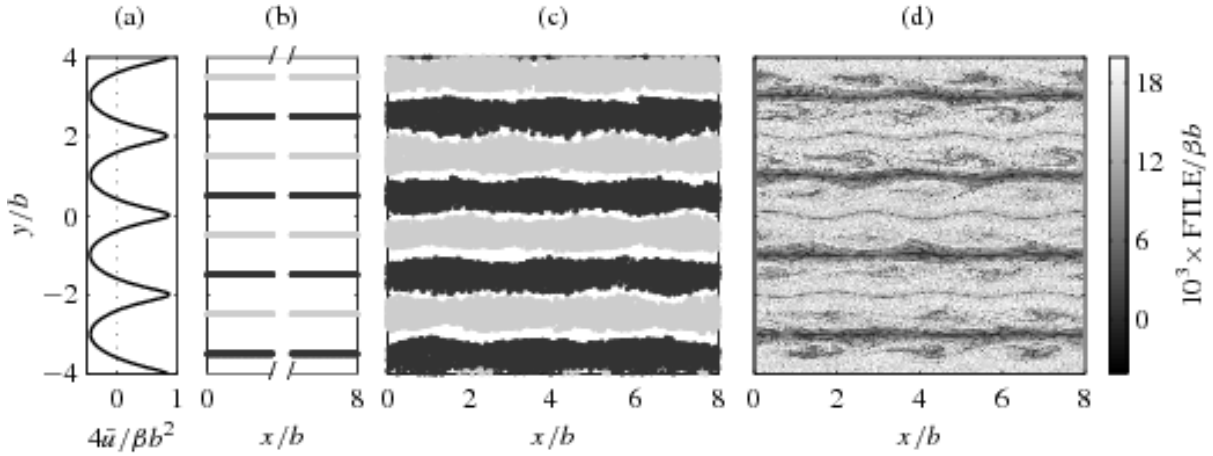

FIG. 3. (a) Zonally averaged zonal velocity $\bar{u}(y)$ at $t = 1$ year. (b) Initial positions $(x(0), y(0))$ of color-coded passive tracers. (c) Positions $(x(\tau), y(\tau))$ of color coded passive tracers at $t = \tau = 1$ year . (d) Finite-time Lyapunov exponent (FTLE) field as a function of initial position computed using a one year integration time interval. The time-dependent velocity field whose final state is shown in Fig. 2 was used to construct (a), (c) and (d).

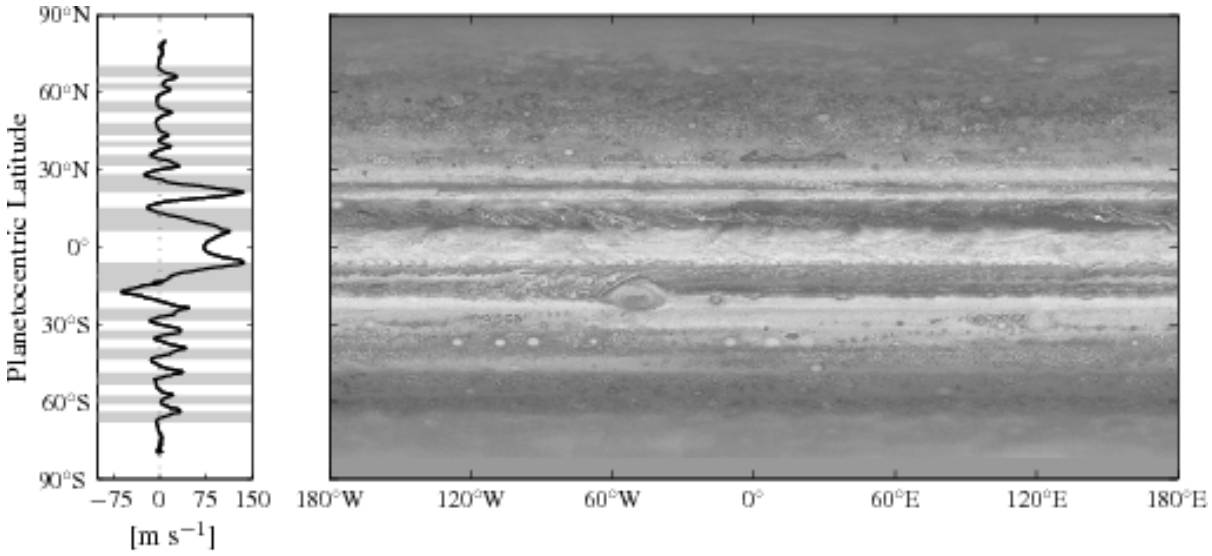

FIG. 4. (left panel) Zonally-averaged zonal wind speed as a function of latitude on Jupiter at the cloud top level as inferred from images taken in December 2000 by the *Cassini* spacecraft (Porco et al. 2003). Gray and white zonal bands indicate belts and zones, respectively. (right panel) Near instantaneous visible band image of Jupiter constructed from images taken by the *Cassini* spacecraft in December 2000. Note that many features of Jupiter's weather layer that are not seen in this image may be revealed by radiative transfer analyses outside of the visible band of the electromagnetic spectrum. NASA image PIA07782 (PIA images are available at NASA's Planetary Photojournal website http://photojournal.jpl.nasa.gov).

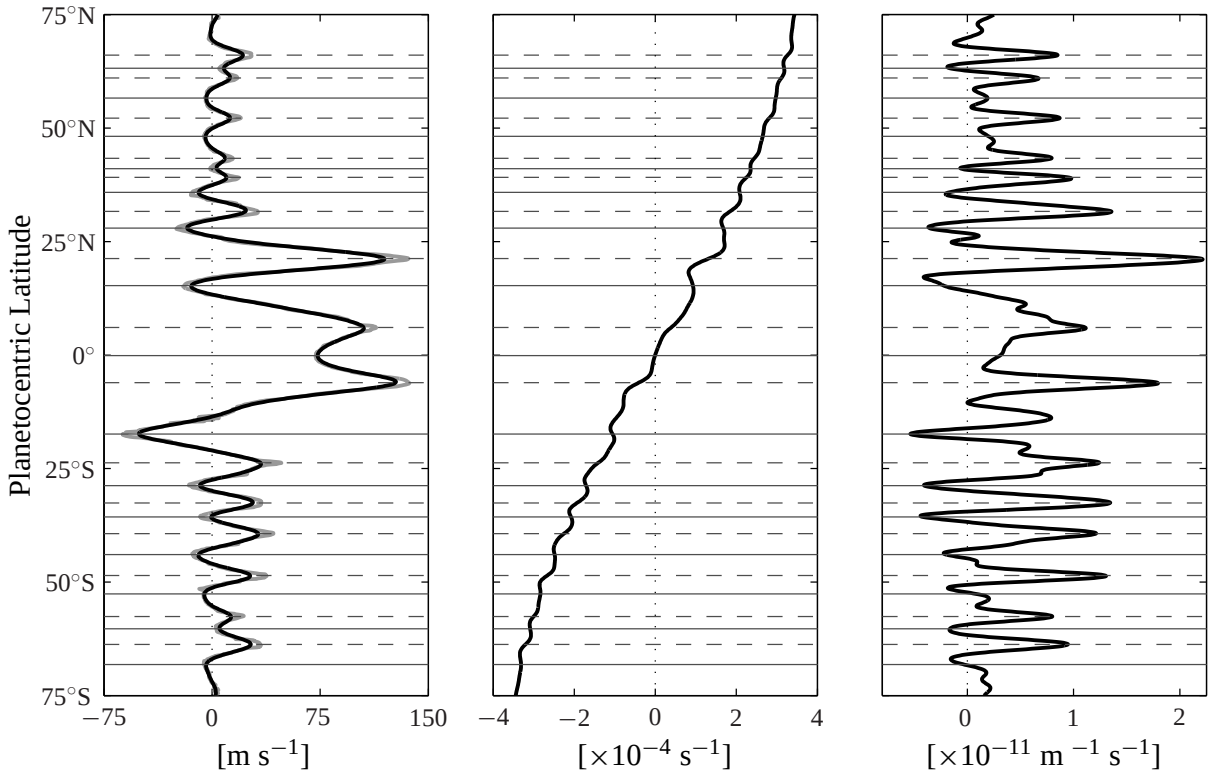

FIG. 5. Meridional distribution of zonally-averaged zonal wind $u_0(y)$ (left panel), zonally-averaged potential vorticity $q_0(y)$ (center panel), and zonally-averaged potential vorticity gradient $q_0'(y)$ (right panel) in Jupiter's weather layer based on *Cassini* data. Both unsmoothed and smoothed wind profiles are plotted; the smoothed wind profile was used to compute $q_0(y)$ and $q_0'(y)$. Solid and dashed horizontal lines are drawn at the latitudes of the cores of westward and eastward jets, respectively. Note that large positive values of $q_0'(y)$ coincide with the cores of eastward jets. A spherical planet (rather than a β-plane, which is used elsewhere in this paper) was assumed to compute the $q_0(y)$ and $q_0'(y)$ structures shown.

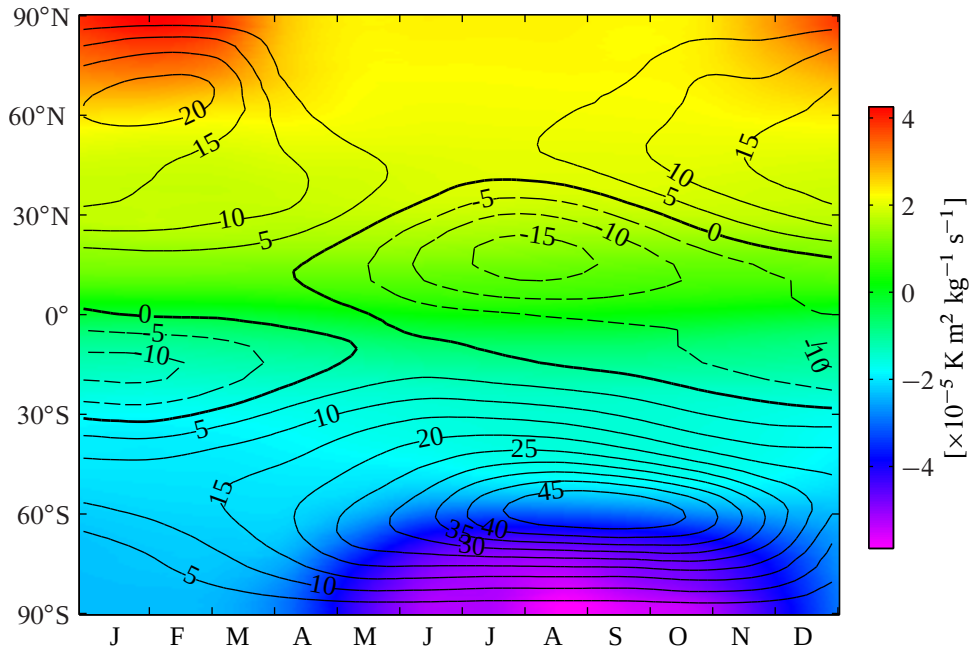

FIG. 6. Seven-year (1992–1998) monthly average of zonally-averaged zonal wind and potential vorticity on the 460 K isentropic surface based on the ERA-40 reanalysis product. Contours show zonal winds in meters per second. Solid and dashed contours represent eastward and westward flow, respectively. Colors indicate Ertel's potential vorticity.